J. Fluid Mech. (1979), *vol.* 93, *part* 1, *pp.* 1–27
Printed in Great Britain

Measurements in subsonic and supersonic free jets using a laser velocimeter

By JARK C. LAU, PHILIP J. MORRIS
Lockheed-Georgia Company, Marietta, Georgia

AND MICHAEL J. FISHER
Institute of Sound and Vibration Research,
University of Southampton, England

(Received 22 August 1977 and in revised form 28 November 1978)

Velocity measurements in a 51 mm diameter turbulent jet are presented. The measurement programme is conducted in two parts. The first part is devoted to the validation of laser velocimeter (LV) data. This consists of comparative measurements with the LV and a hot-wire anemometer. The second part consists of a survey of the jet flow field at Mach 0·28, 0·90, and 1·37 under ambient temperature conditions. Radial and centre-line distributions of the axial and radial, mean and fluctuating velocities are obtained. The distributions indicate a decrease in the spreading rate of the mixing layer with increasing Mach number and a corresponding lengthening of the potential core. The results further indicate that these two parameters vary with the square of the jet Mach number. Radial distributions collapse when plotted in terms of $\sigma\eta^*$, where $\sigma = 10{\cdot}7/(1-0{\cdot}273\,M_J^2)$ and $\eta^* = (r-r_{0{\cdot}5})/x$. This is true for distributions in planes located as far downstream as two potential core lengths. The collapsed data of mean velocity can be approximated by a Görtler error function profile:

$$U/U_J = 0{\cdot}5\,[1-\mathrm{erf}\,(\sigma\eta^*)].$$

Centre-line distributions at various Mach numbers also collapse if plotted in terms of x/x_c, x_c being the potential core length. A general equation for the collapsed data of mean velocity is given by: $U/U_J = 1-\exp\{1{\cdot}35/(1-x/x_c)\}$, for the range of Mach numbers 0·3–1·4, where $x_c = 4{\cdot}2+1{\cdot}1\,M_J^2$.

1. Introduction

In an attempt to understand more fully the noise generating mechanism in round jets, considerable effort has been expended in the measurement of various flow parameters and the study of how these quantities vary with jet flow conditions. As a result of this effort, the knowledge of the jet structure has substantially improved over recent years (e.g. Mollo-Christensen, Kolpin & Martucelli 1964; Bradshaw, Ferris & Johnson 1964; Davis 1966; Laufer 1974; Lau & Fisher 1975).

In these studies, the hot-wire anemometer has featured very prominently, primarily because it is able to measure not only the mean but also the fluctuating velocities. However, due to its fragile nature, its use is generally restricted to regions where the flow conditions are not very severe. Thus, most of the work has been performed in

0022-1120/79/4244-6770 $02.00

low Mach number and low temperature jets. In the context of jet noise, however, the problem has been more pressing at the very high Mach numbers where present methods of noise reduction (such as with the high bypass engine) are not applicable. This has called for an experimental effort along lines and on a scale similar to that conducted previously on low Mach number jets using hot-wires, and necessitated the development of a high Mach number instrument with the same versatility as a hot-wire. It was partly due to this that a number of remote-sensing optical instruments has been developed since the mid 1960s and the laser velocimeter is one of them.

Most of the previous measurements in high-speed jets have concentrated on the distributions of the axial mean velocity obtained with total pressure tubes. These measurements have furnished information on such parameters as the spreading rates of the high shear regions of the jet and have given useful insights on these regions. The results of these earlier studies have been brought together by Birch & Eggers (1972) and the salient features of the data are summarized in their review paper. They noted a significant scatter in the observed spreading rate of the jet shear layer from the different studies. However, the data all possess one trend, and that is, the jet spreads less rapidly as the Mach number is increased.

Other studies have been concerned with the decay of the jet centre-line velocity. Witze (1974) made use of Kleinstein's (1964) theoretical formulation to derive from the experimental results of thirteen studies, an empirical relationship for the decay in the centre-line velocity for varying Mach numbers, and showed that the length of the potential core of the jet increased with increasing Mach number.

Some turbulence intensity data have become available more recently as a result of measurements with laser velocimeters. Knott & Mossey (1975) studied a free jet at Mach 0·5 and 1·55, and Morris (1976) studied jets at Mach 0·47 to 1·67 issuing into a parallel stream. In both cases, the measurements were restricted to only the axial component of velocity, and were carried out without the full advantage of a Bragg cell in the laser system. Barnett & Giel (1976) had the use of a Bragg cell and measured the axial and radial velocity components, but their work was limited to a jet speed of 121 m/s.

In the present study, the aim is to build upon the knowledge which has so far been acquired on high speed jets as a result of the earlier mean flow measurements and to extend the scope of the available data to include the mean radial velocity and the fluctuating axial and radial velocities. For this purpose, a two-vector laser velocimeter is used. This permits measurements of the velocity in two orthogonal directions.

The measurements are conducted at jet Mach numbers of 0·28, 0·9 and 1·37. In each case, the jet is maintained at the temperature of the ambient air. Since the laser velocimeter is still in its infancy, a special effort is made at Mach 0·28 to assess the validity of the measurements by comparison with corresponding hot-wire measurements. This forms the first phase of the study. The measurements include (*a*) mean velocity, (*b*) turbulence intensities, (*c*) probability density distributions of the fluctuating signals, and (*d*) spectra.

In this report radial distributions of the flow characteristics are presented to illustrate in general how they change over the jet flow field. An attempt is made to achieve some degree of collapse of these results so that the effects of Mach number may be more clearly displayed. Results of the variation of the flow quantities on the jet centre-line are also presented to reinforce some of the insights gained from the

radial distributions. Finally, conclusions regarding Mach number effects are reviewed, and an attempt is made to obtain empirical formulations for Mach number effects.

2. Experimental set-up

2.1. *Air supply*

Dry air is supplied from a plant compressor facility at 2 MN/m^2. Upstream of the jet facility, the air line divides into two branches, one going to a sudden expansion burner, and the other leading directly to the mixing chamber, which is also connected to the outlet from the burner. The desired plenum temperature is achieved by an appropriate mixture of the hot and cold air streams. The plenum is 0·28 m in internal diameter and about 3 m long. A circular baffle, the size of the inlet pipe (0·10 m), is located in the plenum, at about 0·20 m from the inlet. It is mounted concentric with the plenum and serves to decelerate the flow entering the plenum and to disperse the fluid to the outer radius. No acoustic treatment is provided inside the plenum, and no further screens or baffles are incorporated.

For the subsonic experiments, a converging nozzle is attached to the exit of the plenum chamber. The converging-diverging nozzle used for the supersonic experiment is designed by the method of characteristics and the test condition is chosen on the basis of Schlieren pictures taken of the jet under varying plenum pressures and the pressure which results in an essentially shock-free jet. The nozzles have an exit diameter of 51 mm, and are contoured so that the jet emerges parallel to its own axis in each case.

2.2. *The hot-wire anemometer and ancillary equipment*

A DISA 55D01 constant-temperature anemometer is used in conjunction with a DISA 55D10 linearizer. The probe is a single-wire type and is made from 5 μm tungsten wire. The d.c. level of the anemometer output is measured with a Hewlett–Packard Digital Voltmeter and the r.m.s. level with a B & K 2416 Electronic Voltmeter. The probability density of the hot-wire signals is obtained by feeding the anemometer signal into the Hewlett–Packard 3721A Correlator, which performs the probability density analysis. The correlator is also used for autocorrelating the hot-wire signals, and spectral densities are obtained by coupling with a Hewlett–Packard 3720A Spectra Display.

2.3. *The laser velocimeter and ancillary equipment*

The laser velocimeter system is shown schematically in figure 1. A 4 W Argon laser is used with a beam splitter/colour separator to generate two pairs of blue, 4880 Å, and green, 5145 Å, beams. These beams are caused to intersect by the optical transmitter system generating a region of orthogonal blue and green fringes. One set of fringes is arranged normal to and the other set parallel to the jet axis. An optical receiver system is focussed onto this small ellipsoidal region, of nominal dimensions 0·3 by 2 mm, which constitutes the measurement volume. The flow passing through the measurement volume is seeded and the green and blue light of alternating intensity, scattered by the particles is detected by the receiving optics, filtered to separate green and blue light, and converted to electronic signals by photo-multiplier tubes.

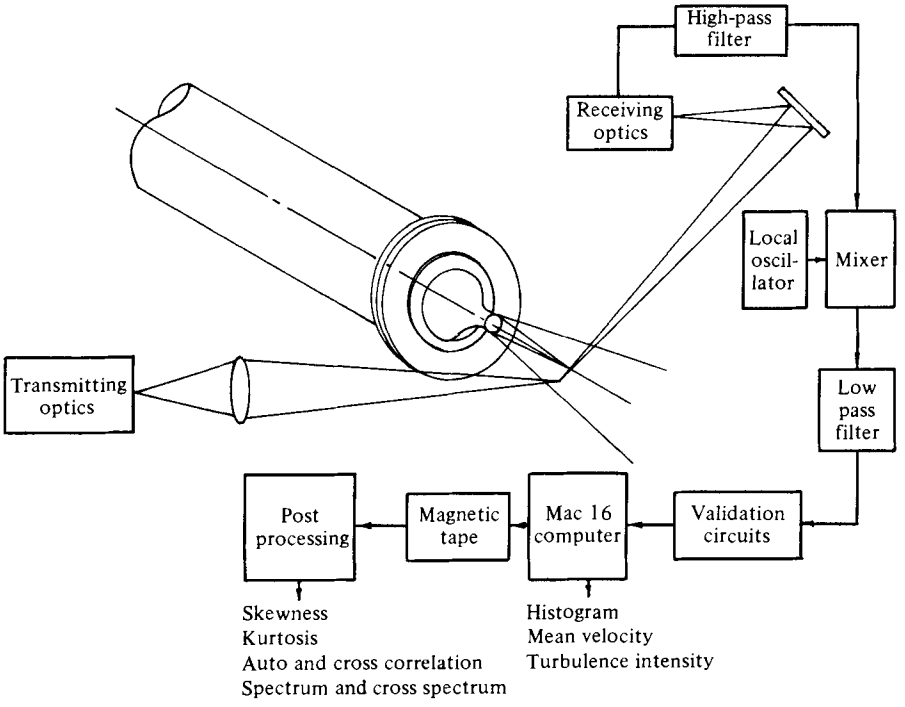

FIGURE 1. Schematic view of the laser velocimeter arrangement.

The high frequency bursts are then processed to provide simultaneous velocity measurements in two orthogonal directions. The optical and electronic processing equipment have been described in detail by Whiffen & Meadows (1974).

In the present set-up, a Bragg cell is incorporated in the transmitting optical system. It is basically an acousto-optical modulator, and when light from one of the two transmitted beams of a given colour passes through it, the light frequency is shifted. The amount of shift is determined by the excitation frequency of the Bragg cell. The effect of this shift in frequency of one of the light beams is to cause the fringe pattern in the measurement volume to move at a constant velocity. Thus a unique frequency burst of scattered light is obtained for particles in the measurement volume having instantaneously positive, zero, or negative velocity.

With the incorporation of the Bragg cell, the signals from each PMT have frequencies ranging from about 40 MHz to over 70 MHz depending on the flow velocity encountered. Since the accuracy of the velocity measurement depends on how accurately the periods of the signals can be determined, the PMT signals are passed through a mixer where they are beaten down to lower frequencies with signals from a local oscillator. The local oscillator frequency is varied during the operation of the LV to ensure that the signals being processed have a range of frequency from 5 to 30 MHz.

The response of the laser velocimeter varies depending on the angle of incidence of the particle with respect to the fringe pattern in the measurement volume. For a system without frequency shifting, the response falls with increasing angle of incidence until an angle where, depending on the number of fringes in the measurement

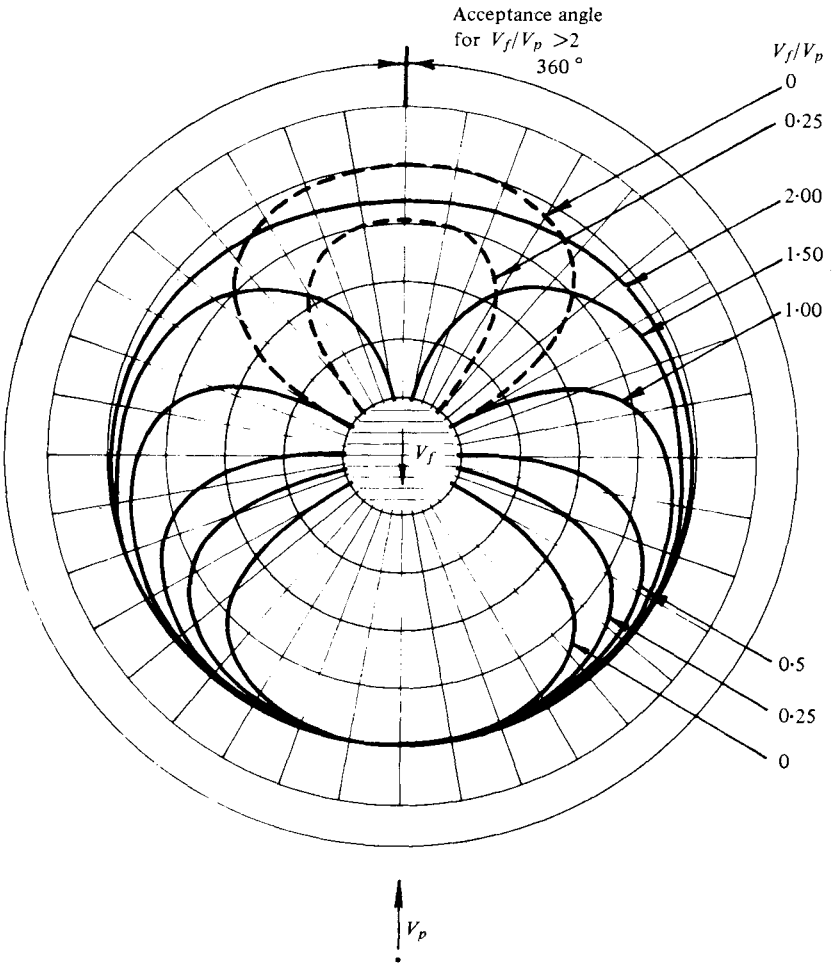

FIGURE 2. Polar response of a moving fringe pattern laser velocimeter.

volume and the number of fringe crossings required for a measurement, no response can be registered by the velocimeter. The angular response of the velocimeter, however, improves with frequency shifting, and the probability of detection of a particle for such a system, $P(\theta)$, may be shown to be

$$P(\theta) = \left[\left\{1-\left(\frac{N/N_T}{\cos\theta + V_f/V_p}\right)^2\right\} \Big/ \left\{1-\left(\frac{N/N_T}{1+V_f/V_p}\right)^2\right\}\right]^{\frac{1}{2}}, \tag{1}$$

where θ is the angle of incidence onto the fringe pattern, N_T is the total number of fringes in the measurement volume, N is the number of fringe crossings required for a measurement, V_f is the effective fringe velocity and V_p is the particle velocity. This probability is shown in figure 2 (Whiffen 1975) for $N/N_T = 0{\cdot}5$ and a number of ratios of fringe to particle velocity. The dashed lines represent ambiguous response characteristics for low fringe to particle velocity ratios. The angle of acceptance has been defined to be the full angle in which particles entering the measurement volume have a 90 % probability of acceptance. For the case shown, therefore, the

acceptance angles for $V_f/V_p = 0$ and $> 2{\cdot}0$ are 80 and 360°, respectively. Care is taken during measurements of a given flow to ensure that the acceptance angle is sufficiently large to encompass the possible angles of incidence of all particles entering the measurement volume.

The flow velocity is determined from the time taken for the particle to intersect eight fringes, or eight cycles of the high frequency bursts. In order to confirm that the signals are valid results from the passing of a single seeding particle through the measurement volume at a given time, the signals are assessed by validation circuits. Tests require that the period, T_N, of N cycles of the signals be related to the period of eight cycles, T_8, by

$$T_8(1-\omega) < 8T_N/N < T_8(1+\omega), \tag{2}$$

where ω is the window of tolerance of the electronic circuit which may be adjusted. In the present system, the signals are passed through two validation circuits in which N is 4 and 5, respectively.

During the measurement period, the instantaneous particle velocities in the orthogonal directions and their time of occurrence are stored on a magnetic tape. This allows the determination of the flow velocity, its statistical characteristics, and auto- and cross-correlation functions from which spectra may be obtained. In order to obtain statistical information about the flow velocity, it is necessary to process the data to remove various biases. For the present type of laser velocimeter, but without frequency-shifting, McLaughlin & Tiederman (1973) have shown that the particle velocity information is weighted by the instantaneous vector velocity magnitude. For one-dimensional unsteady flow it is possible to correct for this biasing by weighting the measured velocity probability distribution by the inverse of the velocity. In this manner the true mean velocity of the flow may be shown to be the harmonic mean of the particle velocity data. If the mean flow direction is normal to a set of fringes and the local transverse turbulence intensity is low, this one-dimensional correction of the measured data has been shown to provide an accurate correction (McLaughlin & Tiederman 1973). If a frequency-shifted laser velocimeter is used, the situation is further complicated and the particle density affects the measurements. Consider an unsteady one-dimensional flow. If the seeding is dilute, the number of realizations will still depend on the instantaneous vector velocity of the particle and the biasing will be essentially unaffected by the introduction of the frequency-shifting. However, if the seeding is heavy, but not so heavy that multiple particles occur in the measurement volume, then the data will be biased depending on the sum of the particle vector velocity and the equivalent velocity of the moving fringes in the measurement volume. The data presented in this work are analysed on the basis of the assumption of heavy seeding. In order to determine the actual biasing involved, an assumption about the relationship between the measured particle velocity and the rate of realizations is necessary since the true time average properties of the fluid are approximated by the sum of the measured velocity and the time between measurements. For example, the expected value of the mean velocity, $\overline{V}'$, is given by

$$\overline{V}' = \frac{1}{T}\sum_{i=2}^{N} V_i \Delta t_i, \tag{3}$$

where V_i is the measured velocity sample and Δt_i is the time between the ith and $(i-1)$th samples. In the laser velocimeter system used in the present study, as noted

above, the time since the last realization is stored. Thus, an unbiased velocity histogram can be obtained by summing the time since the last realization in a particular velocity block, and then normalizing the resulting histogram by the total measurement time. Sample comparisons have been made between results obtained using this processing technique and that employed in the present study and no significant difference was detected. The moments of the flow velocity are readily obtained from the velocity histogram. The processing techniques used to obtain the spectral information are described by Smith & Meadows (1974).

The seeds introduced into the flow are prepared from crushed aluminium oxide mixed with flame-phased silica (CAB-O-SIL). The CAB-O-SIL forms a coating over the particles and samples collected on adhesive surfaces exposed to the flow clearly show an absence of agglomeration (Whiffen & Meadows 1974). The distribution of the particle size has a median of 0·5 μm with an upper two standard deviation size of 1·0 μm. Melling (1971) and Berman (1972) have analysed the response of particles embedded in a turbulent flow based on the particles' motion relative to the flow. From Melling's derivation, it is established by Whiffen & Meadows (1974) that the response of 0·5 μm aluminium oxide particles to a 10 kHz fluctuation in the flow is about 98 % in amplitude with a 12° phase lag.

The seeds are introduced into the plenum by means of a 5 mm tube inserted into the plenum at about 0·3 m from the entrance. To ensure rapid dispersion of the particles over the whole plenum, a row of holes is drilled on the upstream face of the tube. Seeds are also introduced above the jet and allowed to settle into the jet stream. The average rate of *validated* samples detected near the jet axis is about 2000 particles per second.

The transmitting and receiving optical systems are mounted on a frame which is set on a lathe bed. The frame may be moved in three orthogonal directions, and the positioning of the frame has an accuracy which is better than 0·5 mm.

3. Comparison of LV and hot-wire data

One of the main interests of the present study is the range of capabilities of the laser velocimeter system. As an instrument designed for turbulence research, it would need to have the same versatility as the hot-wire. This suggests that it must not only be capable of measuring the mean and turbulence intensity but also the various characteristics which help to describe the turbulence, as for example the skewness of the signals and the spectral distribution of the turbulence.

In this section, the laser velocimeter is used to carry out a series of different types of measurements for the purpose of assessing its capabilities, and the results are compared with corresponding hot-wire measurements made in the same jet. Since hot-wires essentially measure the mass flux of fluid and the laser velocimeter the velocity, the two sets of results are expected to be comparable only when the density remains unchanged. The comparative measurements are therefore carried out at a low Mach number of 0·28. This brings with it the added advantage that the hot-wire would have a longer operational line.

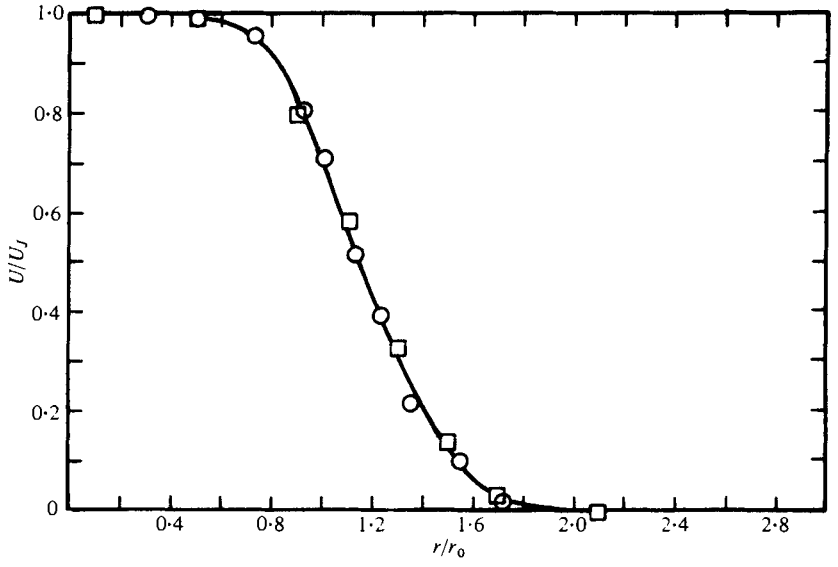

FIGURE 3. Comparison between LV and hot-wire results: U/U_J. ○, LV; □, hot-wire ($x/D = 2$).

3.1. *Mean velocity*

Figure 3 shows radial distributions of the mean axial velocity obtained with the LV and hot wire at an axial station (x) two nozzle diameters downstream of the nozzle. The velocity is normalized by the jet efflux velocity (U_J) and the radial distance by the nozzle radius (r_0). A curve drawn through the LV data may be seen to pass through the hot-wire data also. It is found that for full agreement to be achieved between LV and hot-wire data, it is necessary to ensure that there is some seeding from outside the jet. This is particularly true of results on the outer part of the jet. However, experience has shown that the discrepancy in the middle of the mixing region is not large enough to cause a significant error in such quantities as the maximum velocity gradient or the spreading parameter (σ) which is derived from it.

3.2. *Turbulence intensity*

Figure 4 shows the radial distributions of the axial turbulence intensity. The LV and hot-wire data exhibit the same trends. However, the LV results appear higher in general than those of the hot-wire. The discrepancy in the intensity varies from about 2½ % (representing an error of about 60 % relatively to the hot-wire results) on the jet centre-line to about 3 % (an error of about 20 %) on the lip line. Outside of the lip line there appears to be fairly good agreement. A similar discrepancy exists at other axial stations, and it appears not to depend on the proportion of seeding from the two sides of the jet.

Barnett & Giel (1976) found a discrepancy of the same order in their comparisons between LV and hot-wire data on the inner side of the jet. They attributed this to the arrival in the measurement volume of particles which had velocities which were very different from the local velocity. This had the effect of broadening the velocity probability distribution. However, this does not appear to be the case in the present

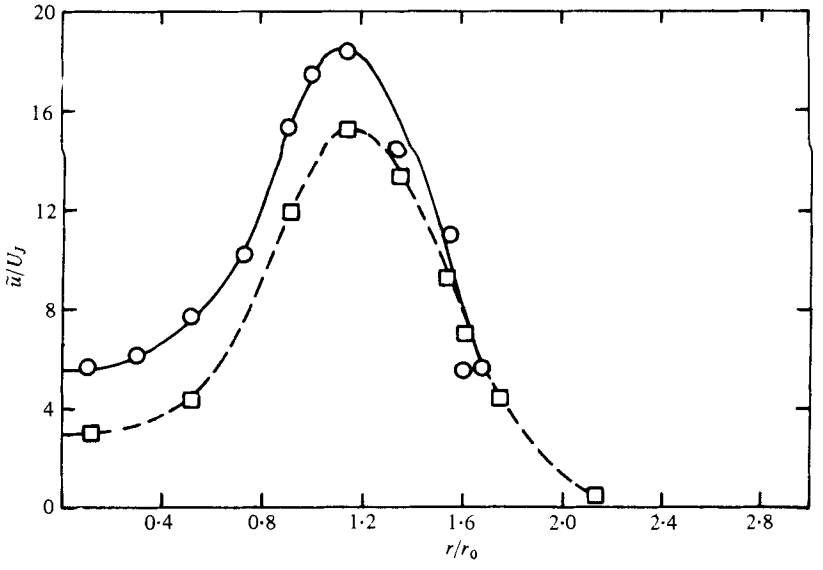

FIGURE 4. Comparison between LV and hot-wire results: $\tilde{u}/U_J$.
○, LV; □, hot-wire (x/D = 2).

study, as for example on the inner side of the jet, seeding comes almost wholly from the inside so that the influence of stray particles from the outer side is negligible and yet the discrepancy is still present. It suggests other possible reasons.

The hot-wire data in figure 4 have been corrected to allow for tangential sensitivity of the hot-wire and the rectification of the signal in accordance with the results given by Champagne & Sleicher (1967) and Tutu & Chevray (1975). On the other hand, the LV data have not been corrected. A review of the obvious sources of error suggests that the LV data are probably a little higher than the correct values. This arises from errors in the resolution of the time information which is used to compute the instantaneous velocities. It is estimated that in the worst situation, the error is about 0·6 % in turbulence intensity. This leaves a discrepancy of about 2–2½ % in turbulence intensity between LV and hot-wire results which cannot be accounted for.

Work is in progress to try to identify the source of the discrepancy. Preliminary results suggest that a substantial portion of the discrepancy may be due to an error in the LV data, and a method has been indicated as to how they may be corrected (Whiffen, Lau & Smith, 1978). The method has also been applied to the data from higher Mach number jets, and it appears that the discrepancy does not deviate significantly when compared with the observed changes due to Mach number variations.

It appears that further corrections may need to be made to the hot-wire data also. Recently, Perry and his colleagues (Perry & Morrison 1971; Samuel & Perry 1974) have found in wind tunnel studies that their measurements of fluctuating velocities were too low when static calibrations were in use. They estimated errors, in some cases, as high as 20 %. Moreover Jerome, Guitton & Patel (1971) have found Disa equipment gives some errors.† It would seem therefore that the correct values for the

† The authors are grateful to a reviewer for pointing this out.

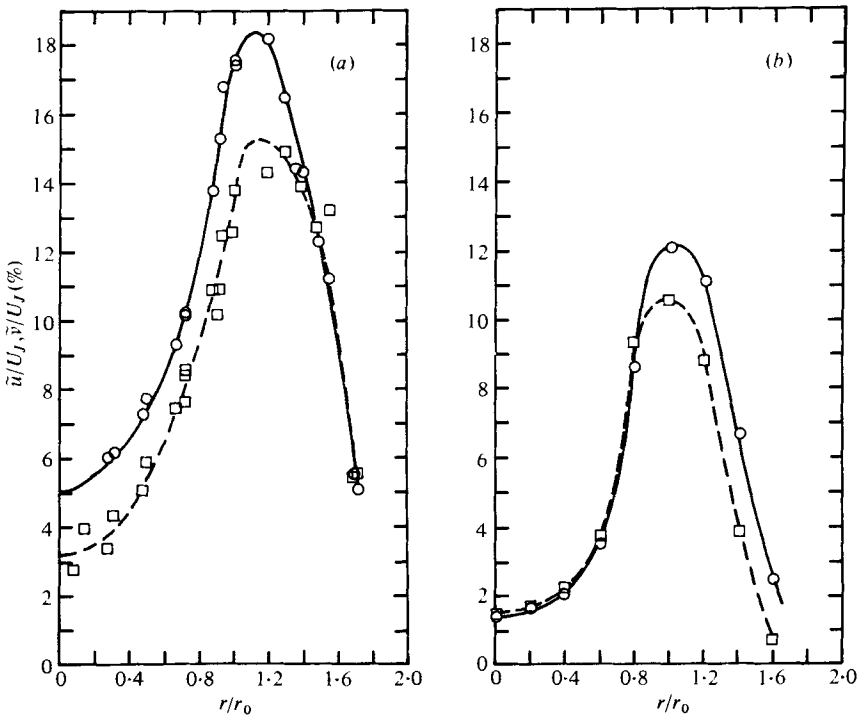

FIGURE 5. Comparison of: ○, $\tilde{u}/U_J$; and □, $\tilde{v}/U_J$ distributions. (*a*) LV, $M_J = 0{\cdot}28$; (*b*) Hot-wire, $M_J = 0{\cdot}17$.

turbulence intensity may lie between the LV and hot-wire data, lying closer to the hot-wire data than those from the LV.

In view of these uncertainties about the corrections, it is decided not to incorporate any corrections to the LV results for the present and wait until more definitive ideas become available.

In the present LV set-up, the radial velocity of the jet is simultaneously measured with the axial velocity. Since the principle used in the LV is the same for the measurement of the two components of velocity, it is expected that the accuracy of the LV measurements of the radial component of velocity would be the same as that in the measurements of the axial component. The radial component of velocity is not measured with hot-wires. An indirect approach is therefore used to assess the data. Figure 5 (*a*) shows a comparison of the turbulence levels of the axial and radial velocity components obtained with the LV. Corresponding data obtained in another two-inch diameter jet using hot-wires (Lau 1971) are shown in figure 5 (*b*). In each case, the radial component of velocity is lower than the axial. In particular, the peaks in the radial velocity turbulence intensity are about three-fourths as high as those of the axial velocity turbulence intensity, suggesting that the discrepancy between LV and hot-wire measurements is probably the same for the radial component as for the axial.

The distributions of the covariance, expressed in terms of $(\overline{u'v'})^{\frac{1}{2}}/U_J$ are shown in figure 6. Also shown are results obtained by Bradshaw *et al.* (1964) using hot-wires. The curves show the same trends, but as before, the hot-wire data tend to be lower. Part of the difference in magnitude between the two sets of results may be attributed

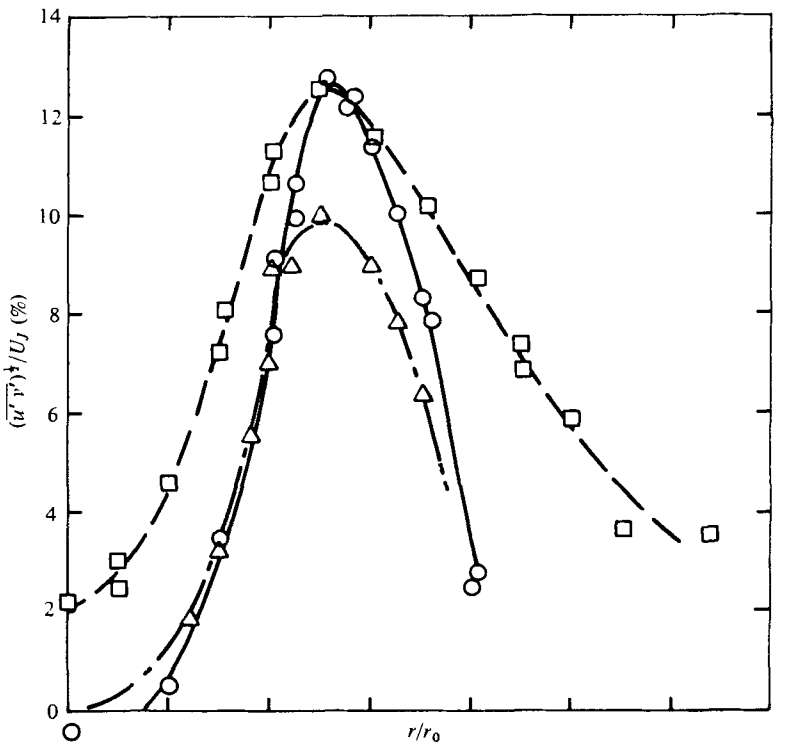

FIGURE 6. $(\overline{u'v'})^{\frac{1}{2}}/U_J$ *vs.* r/r_0. LV results, $M_J = 0{\cdot}28$: ○, $x/D = 2$; □, $x/D = 4$. Hot-wire results (Bradshaw *et al.*, $M_J = 0{\cdot}3$): △, $x/D = 3$.

to differences in the two jets, but this is expected to be small. The discrepancy is of the same order as that found in the axial turbulence. Thus, it appears that the same uncertainty between LV and hot-wire measurement of turbulence intensity exists in the measurements of the Reynolds stress covariance.

3.3. *Probability distributions of axial velocity*

Figure 7 shows the probability distributions of the axial velocity in a plane two diameters from the nozzle. For clarity the corresponding LV and hot-wire results are displaced vertically. The successive figures show the distribution at increasing radii from the centre-line. The LV and hot-wire results at each radial position show similar trends. At $r = 0$, both distributions have a symmetrical form. Moving from the centre-line, the distributions assume a shape with a negative skewness. Still further outward, the distributions become positively skewed. Closer scrutiny of the LV distribution in the outer part of the jet shows that a large portion of the instantaneous velocities is in the negative direction. However, the hot-wire is insensitive to the velocity vector direction and records the negative values as positive. This accounts for the rather steep rise in the probability density near the zero velocity, and demonstrates the need for more careful assessment of previous hot-wire data in this part of the jet.

Figure 8 shows plots of the skewness and kurtosis of fluctuating velocity signals as a function of the normalized radial position. Results by Davies (1966) obtained with

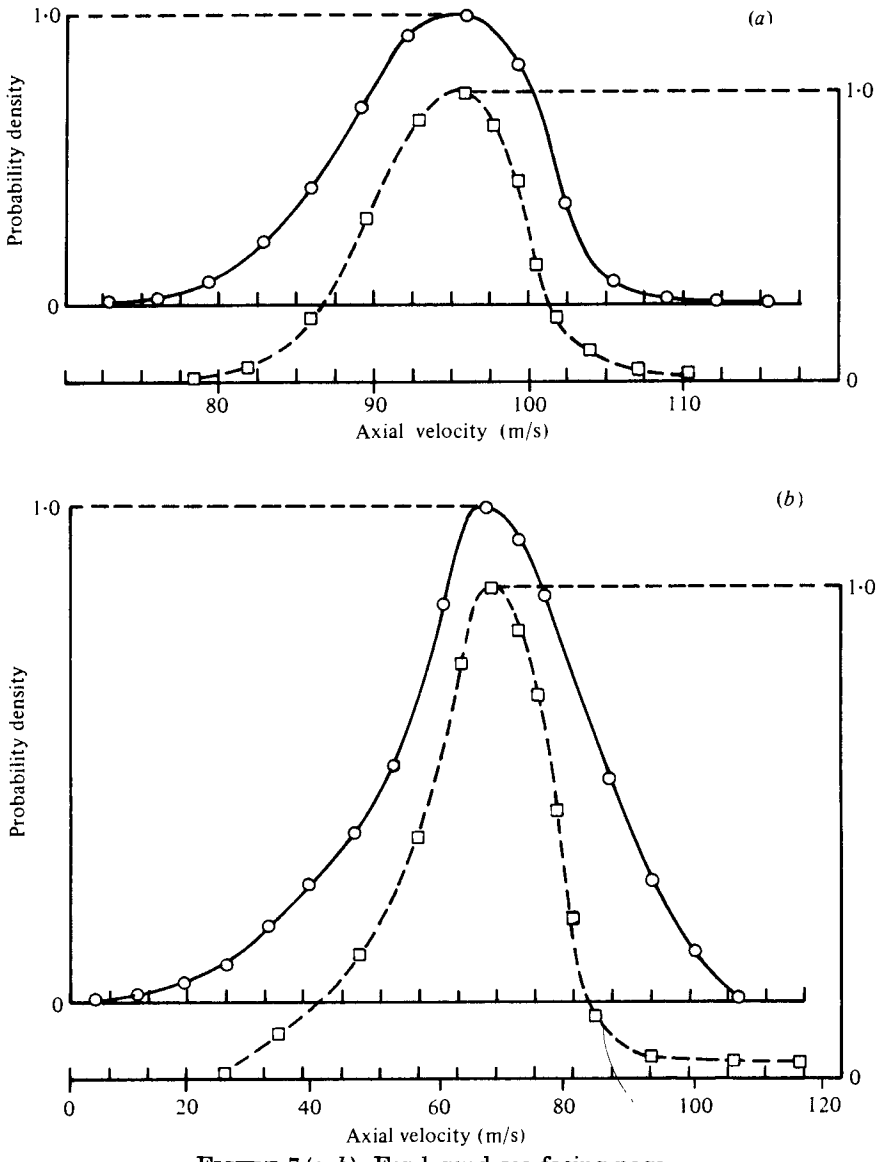

FIGURE 7 (*a*, *b*). For legend see facing page.

a hot-wire anemometer are also shown. The present results exhibit the same trends as those of Davies. A difference however exists in the actual magnitudes at the corresponding η^* locations.

3.4. *Spectra*

Figure 9 shows families of curves of spectra of the axial fluctuations at a number of radial positions obtained with the LV and hot-wire. The power spectral density ordinate is expressed in dB, with an arbitrary reference level. The relative positions of the different curves are however faithfully reproduced. It may be seen that the LV data exhibit more jaggedness. This is believed to be due to a low sampling rate and may be improved with increased seeding rate.

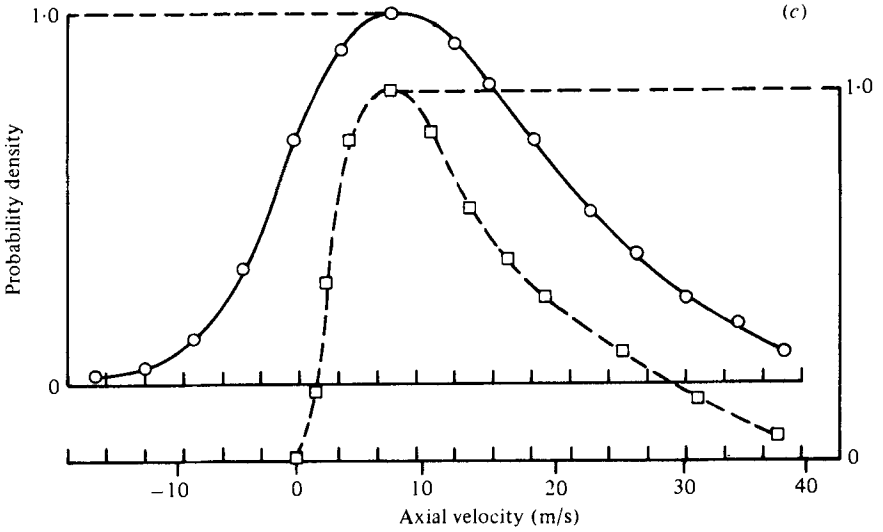

FIGURE 7. Probability density of axial velocity fluctuations, $x/D = 2$. (*a*) $r/r_0 = 0$. (*b*) $r/r_0 = 0{\cdot}8$. (*c*) $r/r_0 = 1{\cdot}4$.

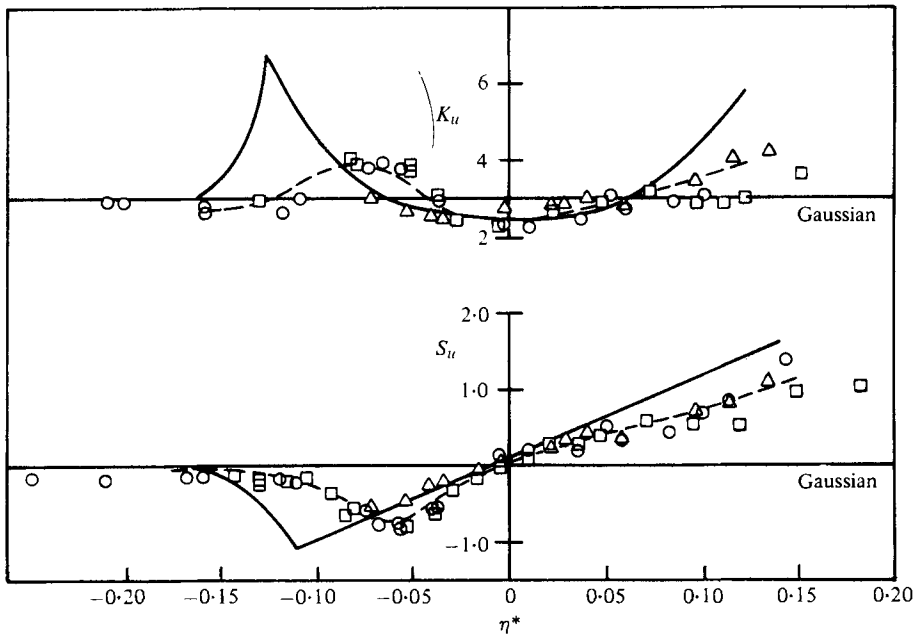

FIGURE 8. Kurtosis and skewness of axial velocity fluctuations: ○, $x/D = 2$; □, $x/D = 4$; △, $x/D = 8$; ——, Davies (25 mm diameter jet).

The two sets of curves exhibit very similar trends. On the jet axis there is a peak in the spectrum. As the radial position is increased, the peak becomes shallower, and by the middle of the mixing region, it disappears. This is consistent with the results given by Bradshaw *et al.* (1964) and Davies (1966) for hot-wire spectra in the jet.

The spectral peak frequency (f) has previously been found to scale with jet speed

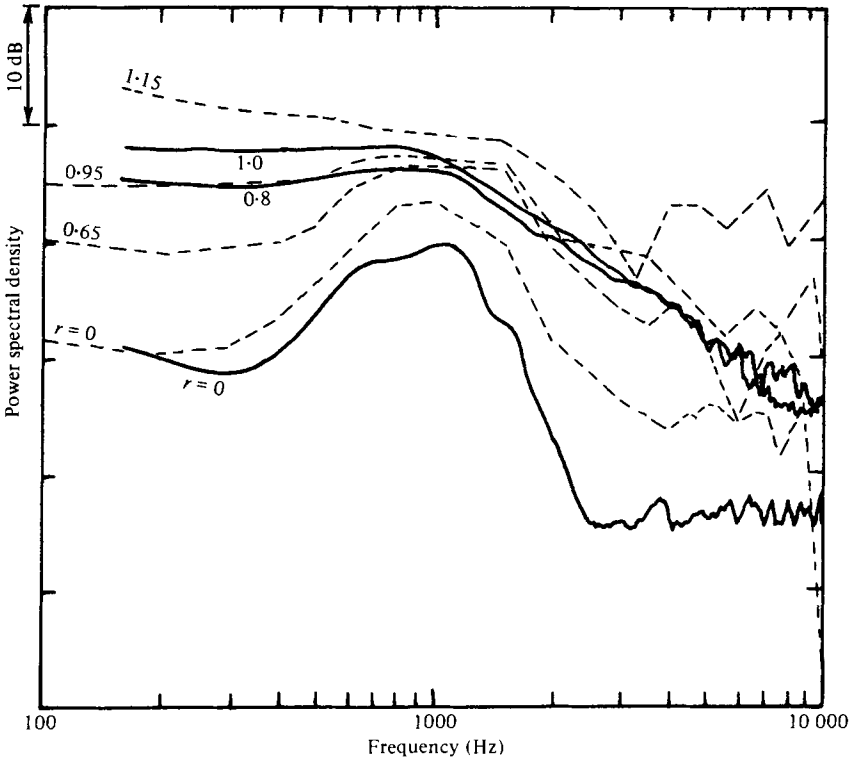

FIGURE 9. Spectra of ---, LV; and ——, hot-wire signals. $M_J = 0{\cdot}28$, $x/D = 2$.

(U_J) and diameter (D), and the present results yield a Strouhal number (fD/U_J) of 0·5. This agrees with previous hot-wire results also. LV spectra at Mach 0·9 give the same value for the Strouhal number.

3.5. *Summary*

This preliminary study has shown that the LV may be used effectively for the measurement of the flow quantities in a turbulent or non-turbulent environment. The distributions of the axial mean velocity measured in the jet agree with those obtained with a hot-wire. The turbulence intensities differ however from corresponding hot-wire measurements by about 2% in intensity across the jet. A similar difference in magnitude is also observed in the velocity covariance. It is still not clear what has caused the discrepancy, and the initial suspicions are on the LV. However, recent work on the hot-wire suggests a possible contribution from the hot-wire also. Since the LV results exhibit basically identical trends as those from the hot-wire, it suggests that in the meantime, the LV may still be used to great advantage for studying turbulent flows especially in regions where the hot-wire cannot be used.

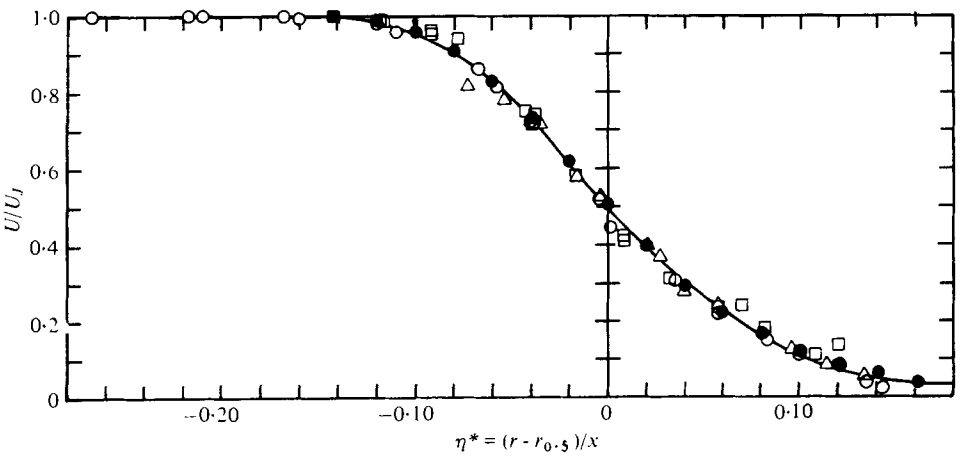

FIGURE 10. U/U_J *vs.* η^*, $M_J = 0{\cdot}28$. x/D: ○, 2·0; □, 4·0; △, 8·0; ●, Görtler (1942). ——, mean fit curve from nine studies of two-diameter shear layers (Halleen 1964).

4. Measurements in the jet flow field

The encouraging results outlined above prompted the next phase of the study which is to observe the trends in the distribution of the various flow quantities as the Mach number is changed in steps from a low subsonic speed to a supersonic speed. The results are presented in the form of radial and axial distributions.

4.1. *Radial distributions*

Mean velocities. Figure 10 shows the mean velocity distributions at three axial stations, at Mach 0·28, plotted in terms of U/U_J and η^*, where U_J is the jet efflux velocity and $\eta^* = (r - r_{0.5})/x$, $r_{0.5}$ being the radial position where the mean velocity is 0·5 U_J and x the distance from the nozzle exit. Two of the axial stations lie within the region where the potential core is known to exist, and one of them lies downstream of the potential core. Also shown are the results of a mean-fit curve computed by Halleen (1964) from the data of nine studies of two-dimensional shear layers, and Görtler's 'exact' solution for the two-dimensional shear layer (1942). The present results collapse very well on these two-dimensional shear layer data.

The collapse of the data at the two upstream stations of the jet may well be expected as the jet has a semblance of a two-dimensional shear layer in the annular region. However, it is interesting that the results eight diameters downstream of the nozzle, which is nearly twice the potential core length, also fall on the same curve. A collapse of circular jet data on two-dimensional shear layer data was also previously achieved by Lau (1971) using hot-wires. These results suggest that the present approach of normalizing the mean velocity (by U_J instead of U on the centre-line) and the radial distance in terms of η^* may be adopted to good advantage in the display of subsequent data. From an experimental point of view, it allows the region of similar mean velocity distributions to be extended beyond the end of the potential core. Moreover, it demonstrates that the simpler theoretical formulations developed for two-dimensional shear layers may be applied to the more complicated three-dimensional situation of a round jet as far as two potential core lengths downstream.

Figure 11 shows the radial distributions of the mean axial velocity at Mach 0·9.

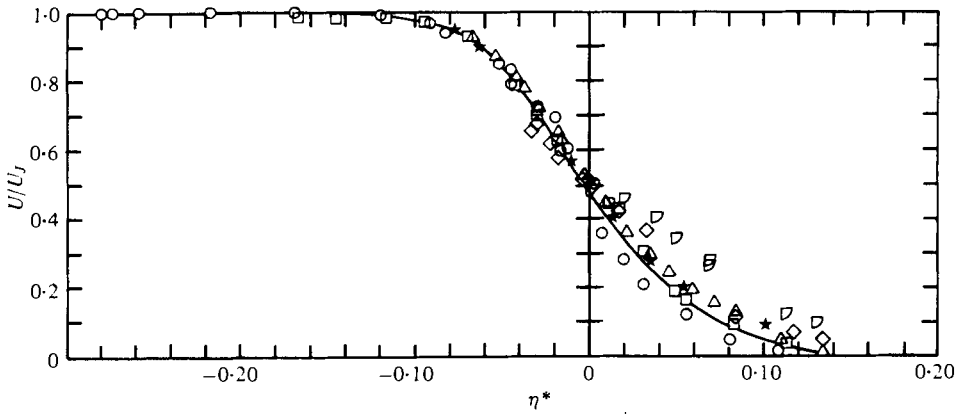

FIGURE 11. U/U_J *vs.* η^*, $M_J = 0{\cdot}9$.
x/D: ○, 2·0; □, 4·0; △, 8·0; ◇, 12·0; ▽, 16·00; ★, Koplin (1964).

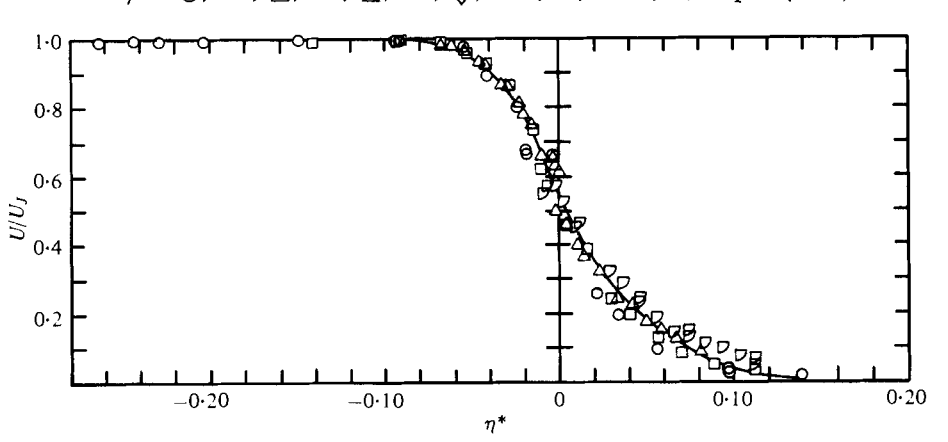

FIGURE 12. U/U_J *vs.* η^*, $M_J = 1{\cdot}37$. x/D: ○, 2·0; □, 4·0; △, 8·0; ▽, 16·0.

The results extend over larger axial distances downstream than for the previous case. In general, there is good collapse of the data on the inner part of the jet (i.e. η^* negative), but significant deviations appear in the outer part. Closer scrutiny reveals, however, that the very large deviations are associated with results at $x/D = 16$. The rest of the results collapse reasonably well so that a faired curve may be drawn through the points. Kolpin's (1964) results from a cold jet are also shown and they produce a similar distribution.

Figure 12 shows the radial distributions at $M_J = 1{\cdot}37$. Good collapse of the data is achieved for even $x/D = 16$. It would seem that the similarity of the mean velocity curves is preserved for a longer distance as the Mach number is increased. This apparently is associated with the increase in potential core length with Mach number as reported by Witze (1974). An estimate based on present results places the maximum distance for similarity a little over twice the length of the potential core. This distance apparently has some significance and may be related to other measurements along the centre-line which will be presented later.

The radial extent of the three faired curves in figures 10–12 is an expression of the relative spreading rate of the shear layer, and the results show a systematic variation as Mach number is increased. At $M_J = 0{\cdot}28$ the shear layer extends from $\eta^* = -0{\cdot}14$

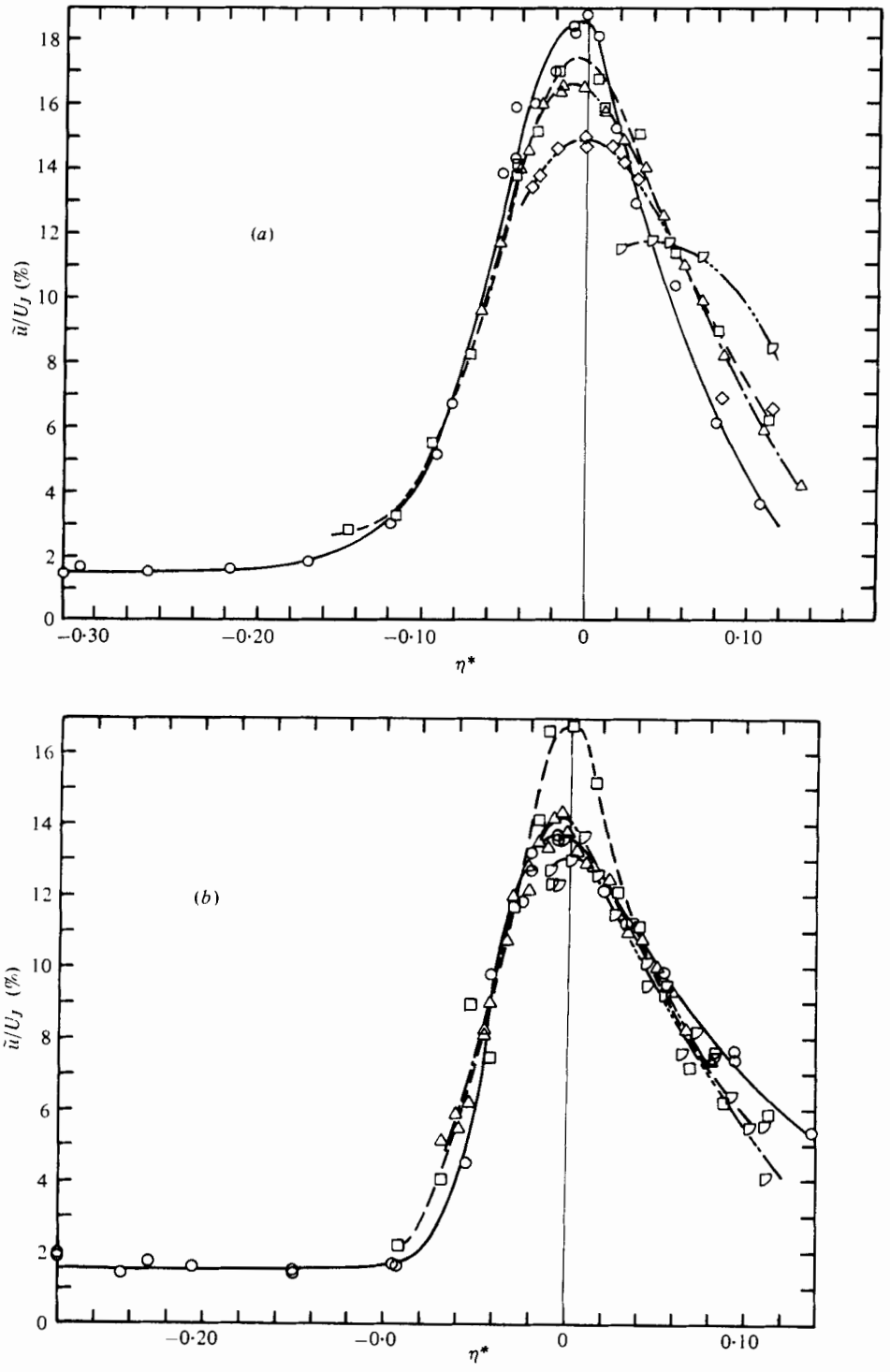

FIGURE 13. $\tilde{u}/U_J$ *vs.* η^*. (*a*) $M_J = 0{\cdot}90$. (*b*) $M_J = 1{\cdot}37$.
x/D: ○, 2·0; □, 4·0; △, 8·0; ◇, 12·0; ▽, 16·0.

to around 0·18 (taking $U/U_J = 0{\cdot}05$ as the lower cut-off point). At $M_J = 1{\cdot}37$ the shear layer extends from $\eta^* = -0{\cdot}08$ to 0·12. Between these two extreme positions, is the curve for Mach 0·9. It is evident that the spreading rate of the shear layer decreases with increasing Mach number. This would agree with trends suggested by earlier investigators.

Turbulence intensities. Figure 13 shows two sets of typical distributions of the axial turbulence intensity. Except for the curve associated with the axial position where the mean velocity distribution does not exhibit similarity characteristics, all the curves show a peak at $\eta^* = 0$. It suggests that within the first two potential core lengths at least, the position for the peak turbulence intensity coincides with the half-velocity point. The decreasing spread of the shear layer with increasing Mach number may readily be observed. The peak values of turbulence intensity do not exhibit any consistent trends, but in general tend to fall with increasing Mach number and downstream distance.

The distributions of the radial turbulence intensity exhibit the same trend, but their magnitudes are generally lower than those of the axial turbulence at corresponding positions.

The peaks of the covariance $\overline{u'v'}/U_J^2$ also lie close to $\eta^* = 0$, and the appearance of the distributions is similar. However, in the inner part of the jet where the potential core is located the values are consistently zero, and in the outer part, the curves tend to intersect the zero axis and assume negative values. The peak values decrease with increasing Mach number and downstream distance.

The variation of the peak values of $\tilde{u}/U_J$, $\tilde{v}/U_J$, and $\overline{u'v'}/U_J^2$ is summarized in figure 14.

4.2. *Flow characteristics along the jet centre-line*

Figure 15 shows the axial distribution of the mean velocity on the jet axis for different Mach numbers. The results exhibit a consistent trend in which the curves move downstream as the Mach number is increased. This shift in the curves agrees with the suggestion of a lengthening potential core.

The results of Knott & Mossey (1975) are also shown. They generally fit into the pattern which is suggested in the present set of results. For instance, their results for a cold jet at $M_J = 0{\cdot}5$ lie between the curves for the isothermal jets of $M_J = 0{\cdot}28$ and $M_J = 0{\cdot}9$. Their results for the heated jet at $M_J = 1{\cdot}55$ lie downstream of all the results presented so far, which is reasonable.

Witze (1974) has proposed an equation for the mean velocity distribution on the jet centre-line of the form:

$$U/U_J = 1-\exp\{1/\chi\}-1-\exp\{\alpha/(1-x/x_c)\} \quad \text{for} \quad x > x_c, \tag{4}$$

where $\alpha = D/(ax_c)$, and 'a' and x_c are dependent on the Mach number and the density ratio between the jet and the ambient conditions. The parameters 'a' and x_c may be determined from experimental results by plotting χ, expressed as $1/\{\ln(1-U/U_J)\}$, against x/D and measuring the slope and abscissa intercept of each of the resulting straight lines. The equations derived for the three isothermal jets are thus:

$$U/U_J = 1-\exp\{6{\cdot}5D/(4{\cdot}1D-X)\} \quad \text{for} \quad M_J = 0{\cdot}28; \tag{5}$$

$$U/U_J = 1-\exp\{7{\cdot}2D/(5{\cdot}2D-X)\} \quad \text{for} \quad M_J = 0{\cdot}9; \tag{6}$$

$$U/U_J = 1-\exp\{8{\cdot}5D/(6{\cdot}4D-X)\} \quad \text{for} \quad M_J = 1{\cdot}37. \tag{7}$$

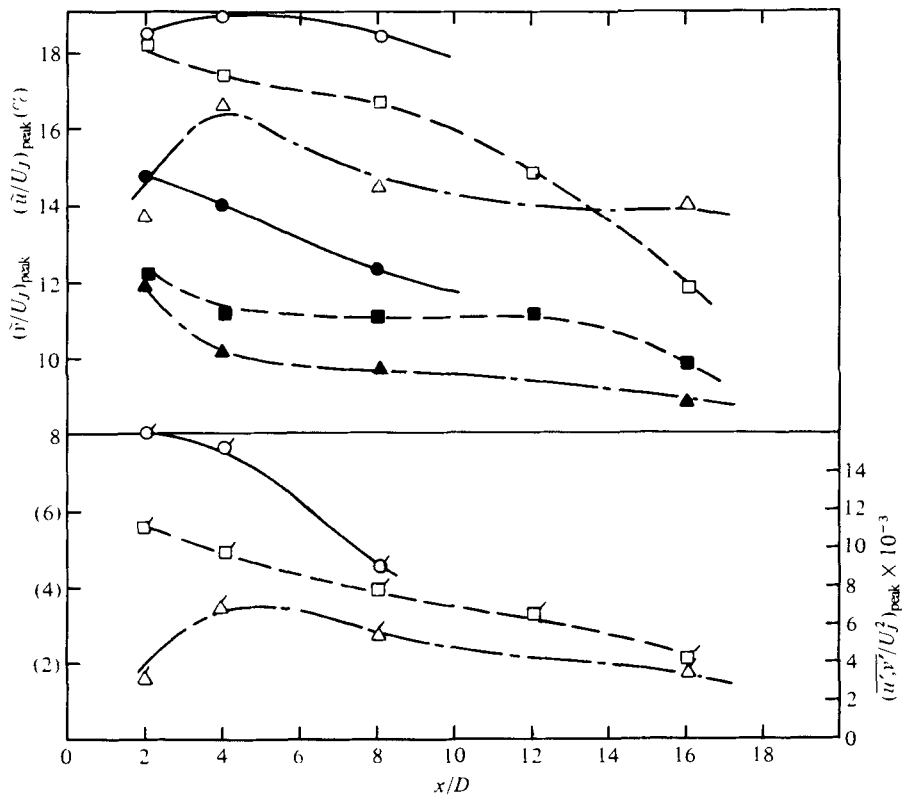

FIGURE 14. Peak values of $\tilde{u}/U_J$, $\tilde{v}/U_J$ and $\overline{u'v'}/U_J^2$ *vs.* X/D.

M_J	$(\tilde{u}/U_J)_{peak}$	$(\tilde{v}/U_J)_{peak}$	$(\overline{u'v'}/U_J^2)_{peak}$
0·28	○	●	◌
0·9	□	■	◻
1·37	△	▲	◬

Curves of these equations are also drawn in figure 15. The curves follow the data points very closely. It appears therefore that the form of equation (4) gives a good representation of how the mean velocity may be expected to vary along the jet centre-line. The parameter x_c gives a direct measure of the potential core length, and the results suggest that isothermal jets at Mach 0·28, 0·9, and 1·37 have potential core lengths of $4{\cdot}1D$, $5{\cdot}2D$, and $6{\cdot}4D$, respectively.

It is found that by normalizing the axial distance by x_c, good collapse of the data is achieved. This is shown in figure 16 which displays the variation of axial mean velocity as a function of x/x_c. Referring to equation (4), the result in effect implies that the term ax_c/D is independent of Mach number. There has been a suggestion by Kleinstein (1964) that this term has a universal value of 0·70 for jets of varying Mach numbers and density ratios. The values obtained in the present study are 0·63, 0·72, and 0·75 for the Mach 0·28, 0·9, and 1·37 jets, respectively.

Figure 17 shows the variation of the axial turbulence intensity on the jet centre-line for varying Mach numbers, plotted in terms of the normalized axial distance x/x_c. The turbulence rises with axial distance, reaches a peak value at about two potential core lengths from the nozzle and subsequently falls. The fall is more gradual

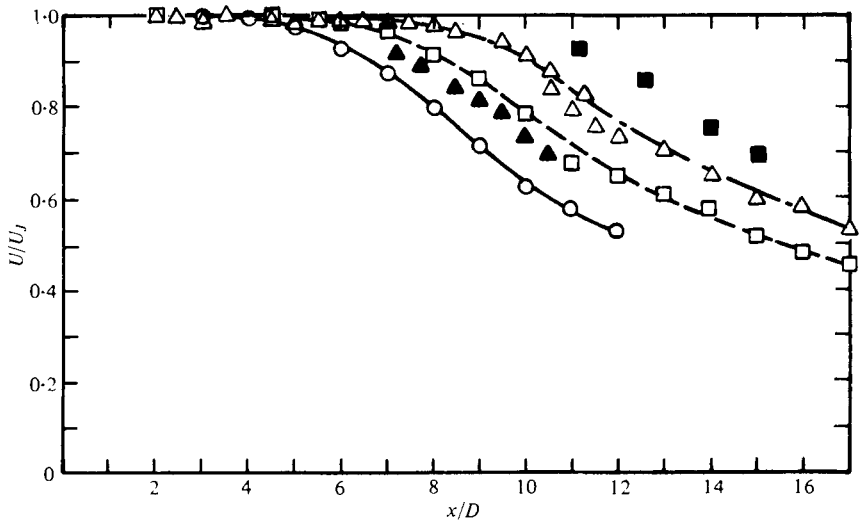

FIGURE 15. Centre-line distribution of U/U_J. M_J: ○, 0·28; □, 0·90; △, 1·37; ▲, 0·5; ■, 1·55 heated (Knott & Mossey 1975); ═══, equations (5), (6), (7).

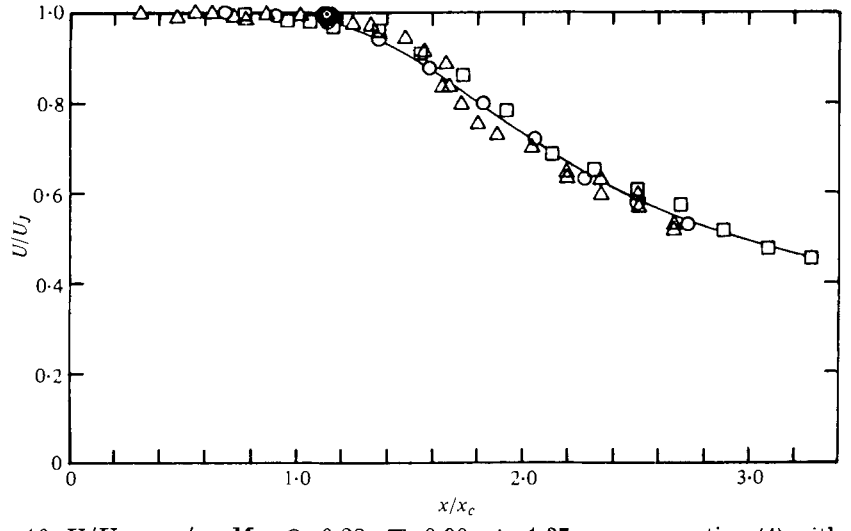

FIGURE 16. U/U_J *vs.* x/x_c. M_J: ○, 0·28; □, 0·90; △, 1·37; ——, equation (4) with $\alpha = 1{\cdot}35$.

than the rise upstream of the peak. The distributions do not fully collapse as in the case of the mean velocity distributions but the fact that they all show a peak at about the same x/x_c suggests that if the intensity levels could be appropriately normalized, a good collapse would be achieved. It was seen earlier that a similar trend prevailed in the radial distributions, and as in those cases, the peak turbulence intensity falls with increasing Mach number.

Figure 18 shows the centre-line distributions of the radial turbulence intensity at different Mach numbers. As in the axial turbulence intensity, the levels rise with axial distance, reaching a peak at about $2x_c$ and subsequently fall. Similar observations may also be made concerning the changing levels with Mach number and the possibility of achieving good collapse of the data if the levels were suitably normalized.

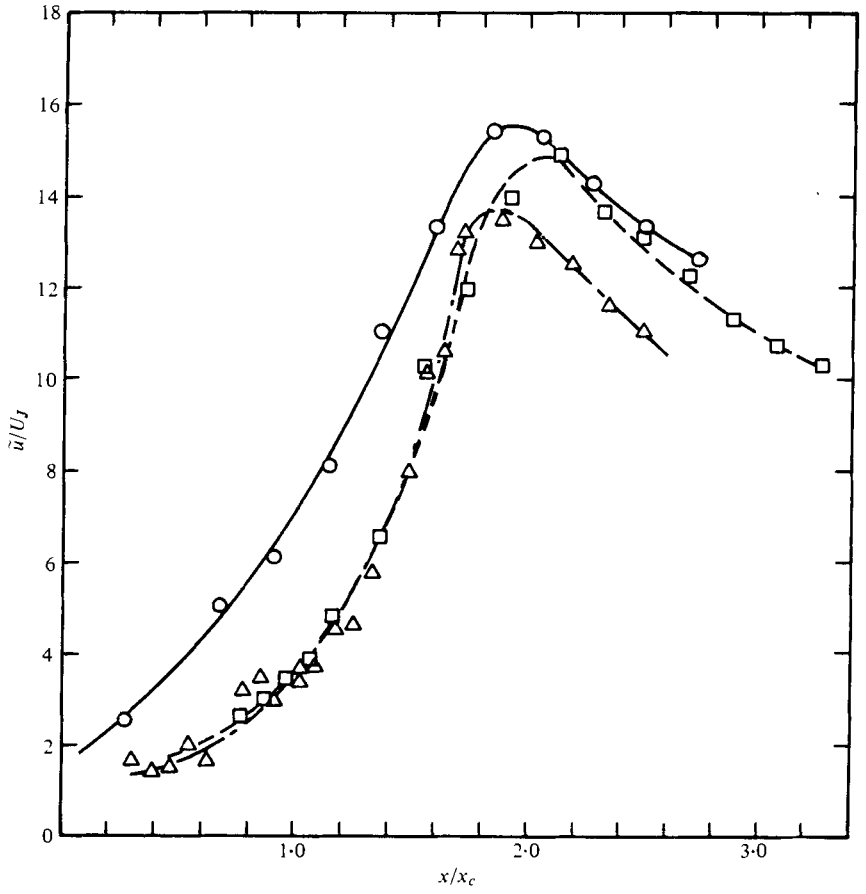

FIGURE 17. $\tilde{u}/U_J$ *vs.* x/x_c. M_J: ○, 0·28; □, 0·9; △, 1·37.

The centre-line distributions of both the mean and fluctuating velocities bring out an interesting aspect about the effect of Mach number on the general flow field. It would seem that when the Mach number is increased, the whole flow field stretches proportionately, and the increase observed in the potential core length is only one of the more apparent manifestation of this general trend. It has been shown by Lau (1971, 1979) that the potential core comes to an end largely because the large-scale vortex pattern within the mixing region converges on the jet centre-line during its travel downstream. An increase in the jet exit Mach number (or more appropriately, jet velocity) would cause an increase in the vortex convection velocity, and if the rate of transverse movement of the vortices does not change substantially as the present results seem to suggest, this would result in the events observed along the jet centre-line being displaced to greater distances downstream. This concept of a proportionate stretching of flow field is also supported by the good collapse evident in the centre-line distributions of the skewness of axial velocity fluctuations shown in figure 19.

4.3. *Mach number effects*

In the previous discussions of the radial and axial distributions of the mean velocity and the turbulence intensities reference was made to some of the more noticeable

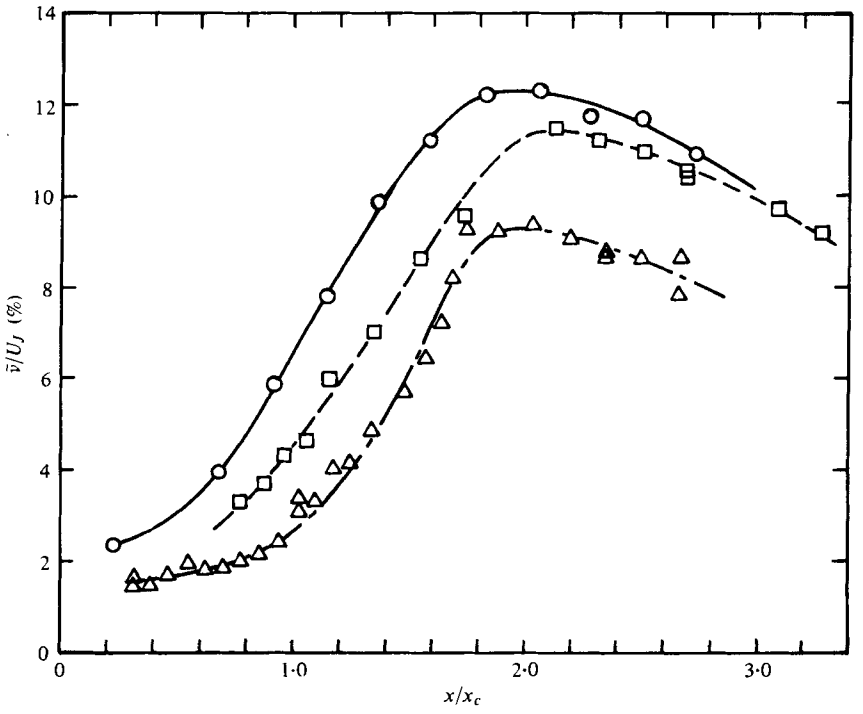

FIGURE 18. $\tilde{v}/U_J$ *vs.* x/x_c. M_J: ○, 0·28; □, 0·9; △, 1·37.

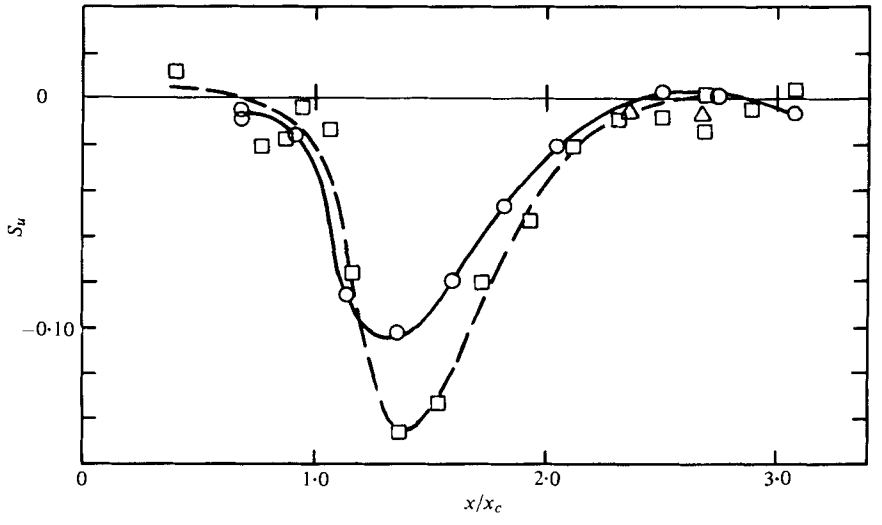

FIGURE 19. Skewness of u' signals *vs.* x/x_c. M_J: ○, 0·28; □, 0·9.

effects of Mach number changes. It was pointed out that the spreading rate of the turbulent shear layer decreased when the Mach number was increased, and that in turn this caused a lengthening of the potential core. It was also brought out that, although no systematic change could be observed, the general tendency was for the maximum axial and radial turbulence intensity in the radial or the axial distribution to fall with increasing Mach number.

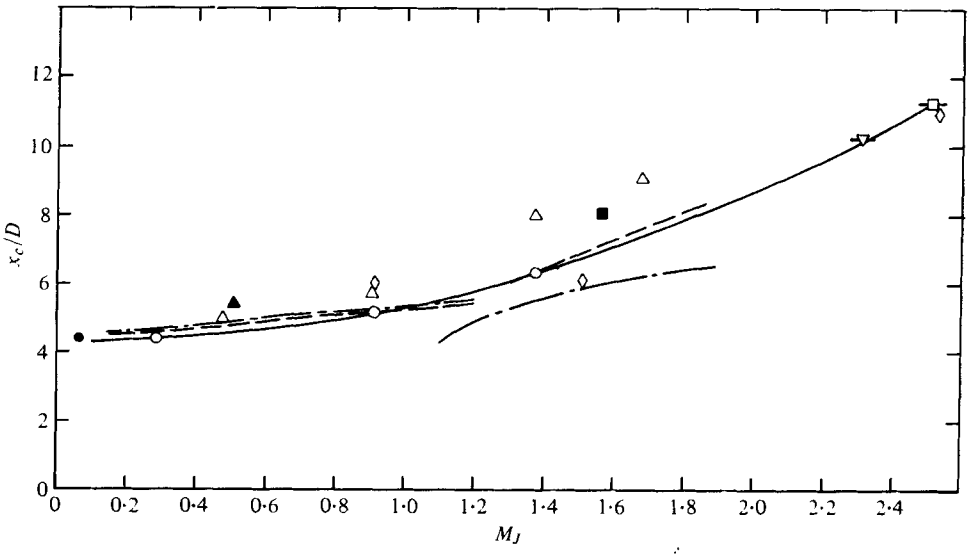

FIGURE 20. x_c/D *vs.* M_J. ○, present results; ——, equation (8); ●, Corrsin & Uberoi; ▲, ■ (heated jet), Knott & Mossey (1975); ◇, Warren; -□-, Potter & Jones; -▽-, Eggers; △ (cold jet), Morris; — — (experimental data), –·– (formulae), Witze (1974).

An attempt is made in this section to quantify some of these observable effects, and possibly to build up with the available data, a set of formulae which may be used to extrapolate results to other Mach numbers.

x_c/D vs. M_J. The variation of the potential core length, x_c, with Mach number, M_J, is shown in figure 20. The potential core length increases monotonically with Mach number over the range measured. The change appears continuous and other results support this observation. The experimental results from eight studies of heated and unheated subsonic round jets and five studies of unheated supersonic jets compiled by Witze (1974) are shown by the dashed line, and they generally pass through the present results for isothermal jets.

Witze used the xperimental results of these 13 studies and derived empirical formulae which give the variation of the potential core length with Mach number. Provision is made in the formulae for density differences between the jet and the ambient medium. The prediction for the subsonic range passes through the data points. However, in the supersonic range, the prediction curve for isothermal jets falls below the experimental results. It is not clear yet what the reason is. However, since Witze's formulation was based on experimental data for cooled supersonic jets, it would appear that an inappropriate account was taken of density effects due to cooling. This matter is being studied at present.

From the available results of isothermal jets from the present study and those of heated and cooled jets from the other studies, it appears that a continuous curve extending from the subsonic to the supersonic range would be a more appropriate representation of changes in potential core length with Mach number. A curve passing through the data points for isothermal jets is drawn based on the equation:

$$x_c/D = 4{\cdot}2 + 1{\cdot}1\, M_J^2. \tag{8}$$

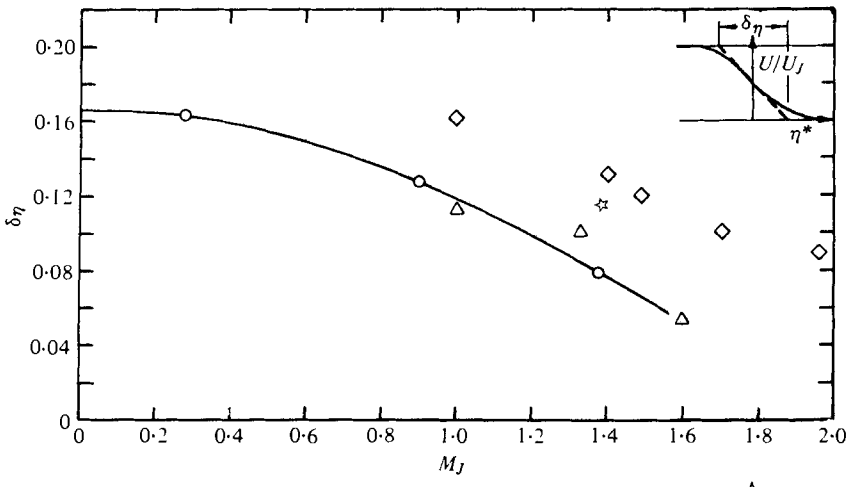

FIGURE 21. δ_η *vs.* M_J. Present results: ○, LV, ——, equation (9); ☆, pitot tube. △, Carey (1954); ◇ (pitot tube), Birch & Eggers (1972).

The curve passes through results of other experimental studies including those of Potter & Jones, Warren & Eggers (see Nagamatsu, Sheer & Horvay 1969) for supersonic free jets. The results of Morris (1976) for jets in a moving stream of velocity ratio 0·1 are also shown. The data lie above the curve which is reasonable since the presence of a secondary stream has been shown to increase the potential core length. The equation appears valid up to Mach 2·5 at least. It suggests that there is a lower limiting value of the potential core length of 4·2 nozzle diameters for $M_J = 0$, and that the value varies little within the lower range of Mach numbers. This is borne out by the many studies of round jets at low speeds.

Spreading rate δ_η vs. M_J. When the radial distribution of the mean velocity is plotted in terms of the normalized parameter η^*, its radial extent gives some measure of the spreading rate of the jet. However, the real extent of the distribution cannot be defined accurately because of the difficulty in determining the cut-off points in the distribution. An approach which has found common usage (e.g. Brown & Roshko 1974) in the definition of the shear layer thickness is to determine the reciprocal of the maximum velocity gradient and to define this quantity as the thickness of the shear layer. In a normalized mean velocity distribution such as that shown in figure 10, the reciprocal of the maximum gradient would give δ_η, which is some measure of the spreading rate.

Figure 21 shows the variation of δ_η with Mach number. Also shown are results of Carey (1954) and other researchers referenced by Birch & Eggers (1972). In all cases, δ_η falls with increasing Mach number. The agreement, however, is best between the present results and those of Carey. These tend generally to be lower than those obtained by the other researchers. It is noted that an interferometer was used by Carey. The discrepancy between the results obtained by optical methods, and those of other researchers using probes suggests the result of a difference in technique, and the possibility of flow restructuring around the instrument when it is introduced into the flow region.

To confirm that a difference really exists between the results from the two techniques, the measurements are repeated in the Mach 1·37 jet using a pitot probe. The

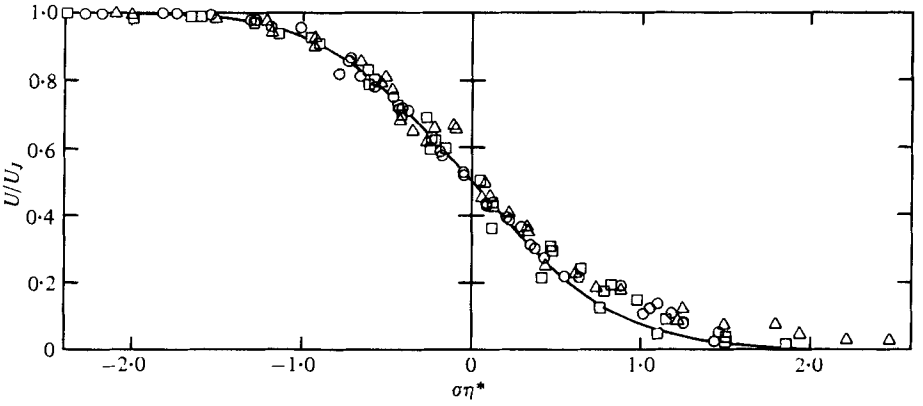

FIGURE 22. U/U_J *vs.* $\sigma\eta^*$ (x/D = 2, 4, 8). M_J: ○, 0·28; □, 0·9; △, 1·37. ——, $U/U_J = 0{\cdot}5\,[1-\mathrm{erf}\,\sigma\eta^*]$.

local Mach number is computed from the ratio of the local static pressure to the local total pressure. (A bow-wave correction is applied to the pitot readings in the supersonic regime.) The resulting spreading rate may be seen in figure 21 to be significantly higher than that obtained with the LV.

The curve drawn through the LV data points for isothermal jets has an equation given by:

$$\delta_\eta = 0{\cdot}165 - 0{\cdot}045\,M_J^2. \tag{9}$$

This curve implies an upper limiting spreading rate of 0·165 which is close to the value of 0·162 indicated by Liepmann & Laufer (1947) for a two-dimensional shear layer at subsonic speed. The equation would probably be applicable only within the range of Mach numbers investigated here, and at higher Mach numbers, the relationship, $\delta_\eta \propto 1/M$, derived by Brown & Roshko (1974) may be more appropriate.

Korst & Chow (1962) have noted that δ_η is related to the better known spread parameter of Görtler by $\sigma = \pi^{\frac{1}{2}}/\delta_\eta$. On this basis, σ may be expressed as a function of the jet Mach number by:

$$\sigma = 10{\cdot}7/(1 - 0{\cdot}273\,M_J^2). \tag{10}$$

Thus, Görtler's solutions for the shear layer become universal solutions for isothermal jets of varying Mach numbers also. The data of figures 10 and 12 are plotted in figure 22 using the radial parameter $\sigma\eta^*$, σ being given by equation (10). It may be seen that Görtler's error function profile [i.e. $U/U_J = 0{\cdot}5(1-\mathrm{erf}\,\sigma\eta^*)$] very closely approximates the collapsed curve, and it is expected that his exact solution would pass through the data as was seen in figure 10.

5. Conclusions

The work has shown that the laser velocimeter is a viable instrument for turbulence research in the high and low-speed range. In its present form, it is not capable of use for conditionally sampled measurements, but otherwise, it has all the capabilities of hot-wire anemometers. It is seen that by using frequency shifting of the optical beams, reversed flows can be detected without ambiguity, and the velocity component in any direction can be measured with the same degree of accuracy as for the main stream.

An unaccountable discrepancy exists between the turbulence intensity measured with the LV and with a hot-wire, but it is still not clear which approach gives a more accurate reading, since the validity of turbulence measurements with hot-wires have recently come into question. This problem remains to be resolved.

Measurements carried out in jets at the same static temperature as the ambient have indicated that the spreading rate of the mixing layer decreases with increasing Mach number. The relationship between the spreading rate δ_η and Mach number is given by:

$$\delta_\eta = 0{\cdot}165 - 0{\cdot}045\, M_J^2$$

or

$$\sigma = 10{\cdot}7/(1 - 0{\cdot}273)\, M_J^2.$$

Radial distributions of the mean velocity for varying jet Mach numbers collapse when plotted in terms of the radial parameter $\sigma\eta^*$. This is true for data obtained as far downstream as two potential core lengths from the nozzle. The data may be approximated by the Görtler error function profile $U/U_J = 0{\cdot}5[1 - \mathrm{erf}\,\sigma\eta^*]$.

A similar collapse of the centre-line distributions of the mean axial velocity is made possible by normalizing the axial distance by x_c, the potential core length, where x_c is given by $x_c = 4{\cdot}2 + 1{\cdot}1\, M_J^2$. The curve passing through the collapsed data is given by $U/U_J = 1 - \exp[1{\cdot}35/(1 - x/x_c)]$.

Radial distributions of the axial and radial turbulence intensity and $\overline{u'v'}/U_J^2$ show characteristic peaks in the middle of the mixing layer. The magnitudes of the peaks fall with distance from the nozzle and increasing Mach number. Centre-line distributions of the turbulence intensities also show peaks. The peaks are located about two potential core lengths downstream, irrespective of the jet Mach number. The magnitudes of the peaks fall with increasing Mach number.

This study was financed by the AFAPL/DOT under contract F33615-73-C-2032. The authors wish to thank Messrs C. B. Reid, M. C. Whiffen, D. M. Smith and R. H. Burrin, and Mrs B. Reagan for their assistance during the study and in the preparation of the report, and the Contract Programme Manager, Dr Harry E. Plumblee, for his encouragement during the course of the study.

REFERENCES

BARNETT, D. O. & GIEL, T. V. 1976 *Arnold Engineering Development Center Report* no. AEDC-TR-76-36, Arnold Air Force Base.

BERMAN, N. S. 1972 *N.A.S.A.* CR-124254.

BIRCH, S. F. & EGGERS, J. M. 1972 *N.A.S.A. Conf. Proc. on Free Turbulent Shear Flows*, vol. 1, *N.A.S.A.* SP-321, pp. 11–40.

BRADSHAW, P., FERRIS, D. H. & JOHNSON, R. H. 1964 *J. Fluid Mech.* **19**, 591–624.

BROWN, G. L. & ROSHKO, A. 1974 *J. Fluid Mech.* **64**, 775–816.

CAREY, B. B. 1954 Ph.D. thesis, University of Maryland.

CHAMPAGNE, F. H. & SLEICHER, C. A. 1967 *J. Fluid Mech.* **28**, 177–182.

DAVIES, P. O. A. L. 1966 *A.I.A.A. J.* **4**, 1971–1978.

GÖRTLER, H. 1942 *Z. angew. Math. Mech.* **22**, 244–254.

HALLEEN, R. M. 1964 A literature review on subsonic free turbulent shear flow. AFOSR-TN-5444, U.S.A.F. (available from DDC as AD606 756).

JEROME, F. E., GUITTON, D. E. & PATEL, R. P. 1971 *Aero. Quart.* **23**, 119.

KLEINSTEIN, G. 1964 *J. Spacecraft* **1**, 403–408.

KNOTT, P. & MOSSEY, P. 1975 *Air Force Aero Propulsion Lab.* TR-76-68, vol. II, pp. 390–416.

KOLPIN, M. A. 1964 *J. Fluid Mech.* **18**, 529–548.

KORST, H. H. & CHOW, W. L. 1962 University of Illinois, Urbana, Mechanical Eng. TN 393–2.

LAU, J. C. 1971 Ph.D. thesis, University of Southampton.

LAU, J. C. 1979 To be published in *Proc. Roy. Soc.*

LAU, J. C. & FISHER, M. J. 1975 *J. Fluid Mech.* **67**, 299–337.

LAUFER, J. 1974 *University of Southern California, Los Angeles, Rep.* USCAE 125.

LIEPMANN, H. & LAUFER, J. 1947 *N.A.C.A. Tech. Note* 1257.

MCLAUGHLIN, D. K. & TIEDERMAN, W. G. 1973 *Phys. Fluids* **16**, 2082–2088.

MELLING, A. 1971 *Imperial Coll. Sci. & Techn. Rep.* ET/TN/B/7.

MOLLO-CHRISTENSEN, E., KOLPIN, M. A. & MARTUCCELLI, J. R. 1964 *J. Fluid Mech.* **18**, 285–301.

MORRIS, P. J. 1976 *A.I.A.A. J.* **14**, 1468–1475.

NAGAMATSU, H. T., SHEER, R. E. & HORVAY, G. 1969 *N.A.S.A. Conf. Washington, D.C., N.A.S.A.* SP-207.

PERRY, A. E. & MORRISON, G. L. 1971 *J. Fluid Mech.* **47**, 765–777.

SAMUEL, A. E. & PERRY, A. E. 1974 *Proc. 5th Australasian Conf. Hydraul. Fluid Mech., Christchurch, N.Z.*, vol. 1, pp. 368–375.

SMITH, D. M. & MEADOWS, D. M. 1974 *Proc. 2nd Int. Workshop Laser Velocimetry*, vol. 1, pp. 27–44.

TUTU, N. K. & CHEVRAY, R. 1975 *J. Fluid Mech.* **71**, 785–800.

WHIFFEN, M. C. 1975 *Proc. Minnesota Symp. Laser Anemometry*, pp. 589–590.

WHIFFEN, M. C., LAU, J. C. & SMITH, D. M. 1978 *Proc. 3rd Int. Workshop Laser Velocimeter.* Purdue University.

WHIFFEN, M. C. & MEADOWS, D. M. 1974 *Proc. 2nd Int. Workshop Laser Velocimetry*, vol. 1, pp. 1–12.

WITZE, P. O. 1974 *A.I.A.A. J.* **12**, 417–418.